Boletim da Sociedade Astronômica Brasileira, **37**, no. 1, 188-192

Identification of dwarf galaxies in dense environments

J. Ibarra[1], A. Cortesi[1,2], S. Torres-Flores[3], & F. Ferrari[4]

[1] Observatório do Valongo, Ladeira Pedro Antônio 43, Saúde, Rio de Janeiro, 20080-090, Brazil
e-mail: jose.ibarra@ov.ufrj.br
[2] Instituto de Física, Universidade Federal do Rio de Janeiro, 21941-972, Rio de Janeiro, Brazil
[3] Departamento de Astronomía, Universidad de La Serena, Raúl Bitrán 1305, La Serena, Chile
[4] IMEF-FURG, Rio Grande, RS, Brazil

Abstract. Dwarf galaxies are key tracers of galaxy evolution, particularly in dense environments where interactions with the intracluster medium and nearby galaxies can influence their structure and star formation activity. Their low luminosities ($-16 < M_r < -10$) and stellar masses ($6 < \log M_\star[M_\odot] < 9$) make them challenging to detect, especially outside the central regions of galaxy clusters. In this work, we present preliminary results from an ongoing project aimed at identifying and characterizing dwarf galaxies in nearby clusters using multiband imaging from the Southern Photometric Local Universe Survey (S-PLUS) and the Dark Energy Camera Legacy Survey (DECaLS), with the goal of investigating how cluster environment influences the structural and evolutionary properties of dwarf galaxies as a function of clustercentric distance. As a first step, we focus on the Fornax Cluster, taking advantage of its extensive S-PLUS coverage and a compiled sample of 330 literature-confirmed dwarfs to validate our detection pipeline. We use `SExtractor` to detect sources across the 12 S-PLUS bands, optimizing background mesh size, aperture definitions, and deblending thresholds to improve the recovery of faint, extended systems. Candidate dwarfs are filtered using apparent magnitude, color, and structural parameters, ensuring consistency with the known dwarf population. We also compute structural and morphological parameters with `Morfometrika` for the subset of objects detected within one virial radius, providing an initial benchmark for interpreting the behavior of candidates in outer S-PLUS fields. These results establish the foundation for extending our pipeline to additional clusters within the S-PLUS and DES footprints.

Resumo. As galáxias anãs são importantes traçadoras da evolução das galáxias, particularmente em ambientes densos, onde interações com o meio intra-aglomerado e com galáxias vizinhas podem influenciar sua estrutura e atividade de formação estelar. Suas baixas luminosidades ($-16 < M_r < -10$) e massas estelares ($6 < \log M_\star[M_\odot] < 9$) tornam sua detecção desafiadora, especialmente fora das regiões centrais de aglomerados de galáxias. Neste trabalho, apresentamos resultados preliminares de um projeto em andamento cujo objetivo é identificar e caracterizar galáxias anãs em aglomerados próximos utilizando imagens multibanda do Southern Photometric Local Universe Survey (S-PLUS) e do Dark Energy Camera Legacy Survey (DECaLS), com o propósito de investigar como o ambiente do aglomerado influencia as propriedades estruturais e evolutivas das galáxias anãs em função da distância ao centro do aglomerado. Como primeiro passo, focamos no Aglomerado de Fornax, aproveitando sua extensa cobertura pelo S-PLUS e uma amostra compilada de 330 galáxias anãs confirmadas na literatura para validar nosso pipeline de detecção. Utilizamos o `SExtractor` para detectar fontes nas 12 bandas do S-PLUS, otimizando o tamanho da malha de fundo, as definições de abertura e os limiares de deblending a fim de melhorar a recuperação de sistemas fracos e estendidos. As candidatas a galáxias anãs são filtradas com base em magnitude aparente, cores e parâmetros estruturais, garantindo consistência com a população de anãs conhecida. Também calculamos parâmetros estruturais e morfológicos com o `Morfometrika` para o subconjunto de objetos detectados dentro de um raio virial, fornecendo um referencial inicial para a interpretação do comportamento das candidatas nos campos externos do S-PLUS. Esses resultados estabelecem a base para a extensão do nosso pipeline a outros aglomerados dentro das coberturas do S-PLUS e do DES.

Keywords. Galaxies: clusters: general – Galaxies: dwarf – Galaxies: photometry

1. Introduction

In the standard cosmological framework of hierarchical structure formation (**?**Davis et al. 1985; White & Frenk 1991; Springel et al. 2005), small systems form first and subsequently merge to assemble more massive galaxies and clusters. In this context, dwarf galaxies are expected to represent the fundamental building blocks of larger structures, providing unique insight into the earliest stages of galaxy formation.

Although intrinsically faint and low in mass, dwarfs play a central role in tracing the assembly history of galaxy clusters. Once they fall into dense environments, their evolution becomes strongly influenced by external processes such as ram-pressure stripping (Jaffé et al. 2018), tidal interactions (Peng et al. 2012), and galaxy harassment (Moore et al. 1996, 1998). These mechanisms can efficiently remove gas and stars, transform their morphology, and quench star formation, making dwarfs excellent probes of environmental processing.

Galaxy cluster environments amplify these effects even further. Being among the densest structures in the Universe, they provide ideal laboratories for studying these mechanisms in action. In such environments, the influence of cluster-centric distance (e.g. Dressler 1980; Boselli & Gavazzi 2014), local galaxy density (Dressler 1980; Peng et al. 2010), and dynamical interactions (Merritt 1983; Gnedin 2003) becomes especially pronounced. Dwarf galaxies—the most numerous and least massive systems ($6 < \log M_\star/M_\odot < 9$, $-16 < M_r < -10$; Venhola et al. 2022), are particularly sensitive to these environmental conditions (Binggeli et al. 1985; Boselli et al. 2006). Their low masses and shallow gravitational potentials make them vulnerable to disruption, yet this same susceptibility allows them to act as powerful tracers of cluster assembly and evolution (Ibata et al. 1994).

Our project aims to investigate how environmental effects in clusters shape the morphological, structural, and stellar population properties of dwarf galaxies. In particular, we ask: Are

the dominant environmental mechanisms primarily driven by cluster-centric distance? And how do tidal interactions and ram-pressure stripping contribute to quenching and morphological transformation?

We focus on dwarf galaxies, which are low-mass, low-surface-brightness systems. Typical dwarfs in our sample have effective radii of $R_e \sim 0.3$–3 kpc, stellar masses in the range $10^{6.5}$–10^9 $M_\odot$, and absolute r-band magnitudes between -10 and -16. Their *low masses and consequently shallow gravitational potentials* (e.g. Peñarrubia et al. 2008; Smith et al. 2013) make them highly susceptible to external perturbations, since even modest tidal or hydrodynamical forces can remove stars and gas or alter their morphology. This sensitivity makes dwarf galaxies excellent tracers of environmental processing in clusters.

2. Data

2.1. Why Fornax? Target Selection Motivation

The Fornax Cluster offers an ideal environment for developing and validating a dwarf galaxy detection pipeline that we can later apply to less studied systems. Its proximity and extensive coverage by both the Southern Photometric Local Universe Survey (S-PLUS) and the Dark Energy Camera Legacy Survey (DECaLS) provide high quality imaging across a wide dynamical range of environments. Multiple existing dwarf galaxy catalogs, including the Fornax Deep Survey (Venhola et al. 2017, 2018, 2022), SMUDGES (Zaritsky et al. 2023), and the ultra compact dwarf catalog of Saifollahi et al. (2021), offer a well-characterized reference population that allows us to test detection performance and photometric reliability.

Crucially, previous surveys have concentrated almost exclusively on the inner $\sim 1\,R_{\rm vir}$ of Fornax. As a result, the outer 3–5 $R_{\rm vir}$ region remains largely unexplored, despite being where environmental effects such as preprocessing, tidal stirring, and gas removal induced by ram-pressure are expected to begin acting on low-mass galaxies. By combining the multi-band information from S-PLUS with the greater depth of DECaLS, our work aims to bridge this gap and extend the study of dwarf galaxies out to the full cluster volume.

Starting in Fornax thus allows us to calibrate our pipeline using a well-studied reference region while simultaneously extending dwarf studies into the poorly explored outskirts. This makes Fornax both a controlled test sample and the natural first step toward a broader environmental analysis across multiple clusters.

2.2. Data and Survey Description

Our analysis combines multi-band imaging from two complementary surveys: S-PLUS (Mendes de Oliveira et al. 2019) and DECaLS (Dey et al. 2019). S-PLUS provides 12 optical bands, enabling precise color-based selection and wavelength-dependent structural measurements, and reaches typical 5σ point-source depths of ~ 21 mag in the $griz$ bands. DECaLS, with deeper grz imaging reaching 5σ depths of $g \simeq 24.0$, $r \simeq 23.4$, and $z \simeq 22.5$ for extended sources, enhances sensitivity to faint and low–surface-brightness systems, particularly in the cluster outskirts.

Together, these datasets provide continuous coverage from the inner $\sim 1\,R_{\rm vir}$ to the outer $\sim 5\,R_{\rm vir}$ of the Fornax cluster, enabling consistent detection and characterization of dwarf galaxies across a wide range of environments. This observational synergy is essential for assessing the performance of our detection pipeline and for preparing its extension to other galaxy clusters.

2.2.1. S-PLUS Observations in the Fornax Cluster

The Southern Photometric Local Universe Survey (S-PLUS) covers ~150 fields across the Fornax region, extending to $\sim 5, R_{\rm vir}$. Of these, 106 fields belong to the S-PLUS Fornax Project (S+FP; Smith Castelli et al. 2024, see orange fields in the top panel of Figure 1), which provides homogeneous 12-band photometry extracted using dedicated `SExtractor` (Bertin & Arnouts 1996) configurations optimized for nearby galaxies. In this first stage, we focus on the 10 central fields ($\lesssim 1, R_{\rm vir}$), which contain 211 of the 330 literature dwarfs. These objects form an ideal sample for calibrating detection thresholds, validating photometry, and tuning the pipeline's performance before extending the analysis to the cluster outskirts.

The 12-band S-PLUS data offer both broad- and narrow-band information that enables efficient color-based separation of stars, galaxies, and background contaminants, while also revealing faint dwarfs with distinct optical signatures. In addition, the multi-band imaging allows us to measure wavelength-dependent structural parameters, such as ellipticity, concentration, Kron radius, and half-light radius, which help identify morphological trends, star-forming regions, and potential tidal features.

2.2.2. DES/DECaLS Coverage

The Dark Energy Camera Legacy Survey (DECaLS; Dey et al. 2019) provides deep grz imaging across the full $\sim 5\,R_{\rm vir}$ extent of the Fornax cluster, covering nearly 5500 imaging bricks (shown in gray on the top of Figure 1). Although offering fewer bands than S-PLUS, its significantly greater depth is essential for detecting extremely faint and low surface brightness dwarfs in the outskirts and for confirming marginal candidates identified in the shallower S-PLUS images.

DECaLS also enables high-quality structural analyses, such as concentration, asymmetry, Sérsic index, and other non-parametric morphology indicators, when processed with external tools such as Morfometrika (Ferrari et al. 2015). These measurements are especially valuable for identifying signatures of environmental processing, including tidal distortions, stellar streams, and asymmetric envelopes.

2.3. Literature Sample and Extended Sample

To calibrate and validate our detection pipeline, we compiled a unified list of previously reported Fornax dwarfs from SMUDGES (Zaritsky et al. 2023), the UCD catalog of Saifollahi et al. (2021), and the dwarf and LSB samples of the Fornax Deep Survey (Venhola et al. 2017, 2018, 2022), yielding 1037 unique candidates. Cross-matching with the S-PLUS Fornax Project catalog (Haack et al. 2024),which provides homogeneous 12-band photometry from dedicated `SExtractor` runs, shows that 330 of these objects are detected in S-PLUS. These constitute our *literature sample*, used to benchmark recovery rates, tune detection parameters, and assess photometric reliability.

The remaining 707 objects form an *extended sample* of systems identified in deeper surveys but absent from Haack et al. (2024). This group is essential for evaluating whether our optimized approach can recover those objects. This division provides a controlled reference set while simultaneously testing the pipeline's ability to push into LSB regimes.

3. Methods

To identify faint dwarf galaxies across the Fornax Cluster, we developed a dedicated detection and characterization pipeline.

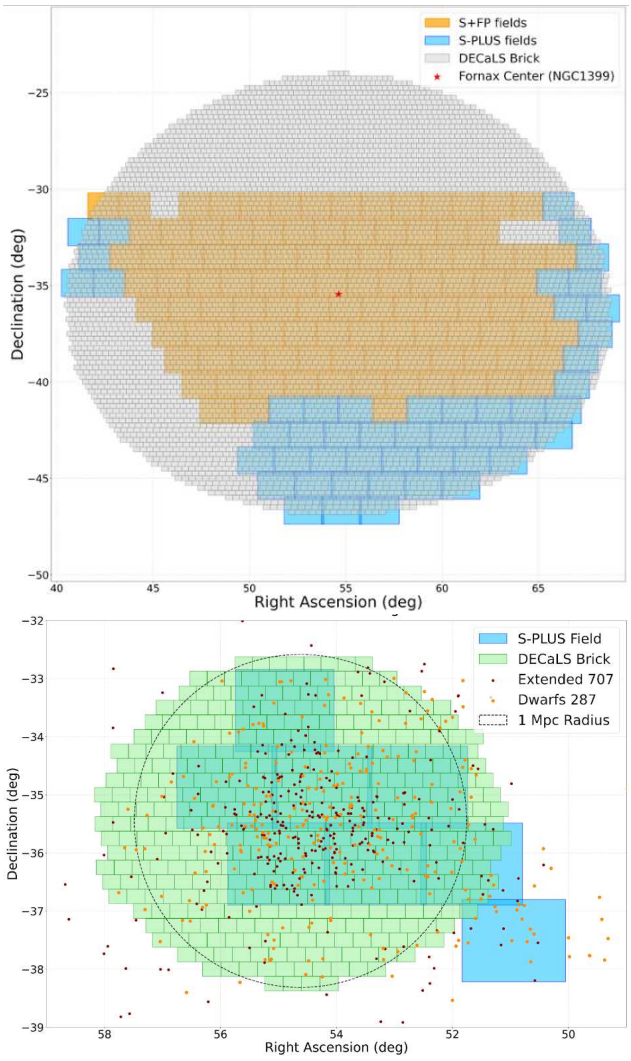

Figure 1. Top: Sky coverage of the S-PLUS and DECaLS fields used in this work. S-PLUS tiles from the S-PLUS Fornax Project (Haack et al. 2024) are shown in orange; complementary S-PLUS tiles are shown in blue. Gray points mark the DECaLS bricks. Bottom: Spatial distribution of the 330 dwarf galaxies compiled from the literature across the S-PLUS/DECaLS footprint.

The workflow includes image preparation, multi-configuration source extraction, performance evaluation, and data-driven post processing. An schematic view can be seen in Figure 2.

3.1. Configuration and Preparation

For S-PLUS, we coadded the *griz* images of each field to build a high signal-to-noise detection frame. This image was used in `SExtractor` dual-mode to ensure consistent 12-band photometry.

For DECaLS, we prepared and coadded the *grz* Legacy Survey images into a separate detection frame, used exclusively for DECaLS-specific `SExtractor` runs targeting faint dwarfs in the cluster outskirts.

3.2. Image Preparation

S-PLUS and DES images were retrieved and used to construct high signal-to-noise detection images. For S-PLUS, we created a detection image by averaging the *griz* broad-band images, which increases the signal-to-noise ratio for faint, low-surface-brightness galaxies. This combined image was used exclusively for source detection in `SExtractor` dual-image mode, while photometry was performed independently in each individual band.

3.3. Detection and Candidate Selection

We applied multiple `SExtractor` configurations to enhance sensitivity to faint and low LSB systems. Each run provided morphological parameters (Kron radius, ellipticity, elongation, second moments) and multi-band photometry. To choose the best configurations, we evaluated their performance through a weighted scoring vector based on:

- **Recall of the literature sample ($R_{\rm Lit}$):** fraction of 330 known dwarfs matched with Haack et al. (2024) within 1″;
- **Extended-sample recovery ($R_{\rm Ext}$):** matches to an additional 707 faint dwarf candidates;
- **Photometric accuracy ($A_{\rm Param}$):** agreement with published photometric and structural measurements;
- **Contamination ($C_{\rm Cont}$):** rate of false positives (foreground stars and background galaxies).

3.4. SExtractor Configuration Grid

Using the `SEWPY` interface, we generated a grid of `SExtractor` setups by varying the detection threshold, convolution kernel, background mesh size, deblending parameters, minimum area, and filtering strategy. Each setup yields a full catalog of morphological measurements and multi-band photometry. The goal is not to find a single "optimal" configuration but to quantify how these choices affect dwarf recovery, contamination, and the stability of structural and photometric parameters.

3.5. Scoring and Selection of Best Configuration

For each configuration, we compute the four metrics above and store them as normalized fractions. These are combined through a weighted score used to rank all setups. The final score is

$$\text{Score} = w_1 R_{\rm Lit} + w_2 R_{\rm Ext} + w_3 A_{\rm Param} + w_4 (1 - C_{\rm Cont}). \quad (1)$$

where $R_{\rm Lit}$ and $R_{\rm Ext}$ are the recalls for the literature and extended samples, $A_{\rm Param}$ is the photometric accuracy of the matched objects of the literature sample, and $C_{\rm Cont}$ is the contamination fraction of stars or other types of galaxies. The configuration with the highest score is then applied to the remaining fields.

3.6. Machine Learning Classification

To further refine the dwarf candidate list, we tested both supervised and unsupervised approaches. In the supervised case, a Random Forest classifier was trained on the literature sample, providing class–membership probabilities and feature importances (size, color, surface brightness, morphology) (identification of objects). For the unsupervised analysis, t-SNE and UMAP projections of the multi-dimensional parameter space were used to visualize the separation between compact dwarfs, diffuse systems, and background contaminants, and to identify outliers (verification or validation of objects).

The Random Forest probabilities, which are shown in Figure 3 display a bimodal distribution. Such bimodality is common in mixed samples and usually reflects a real separation

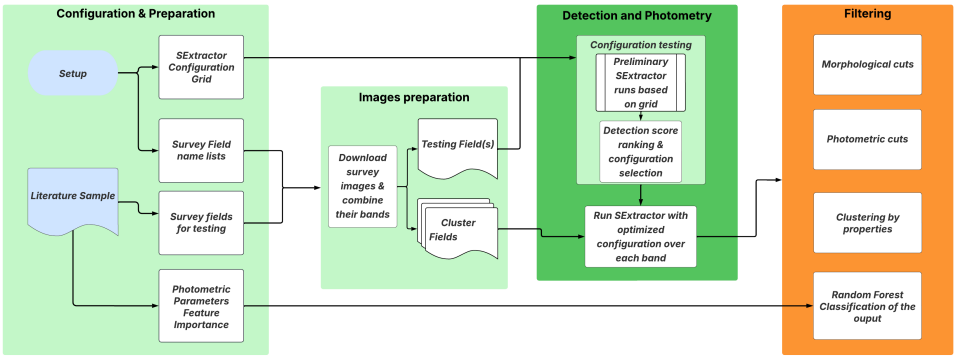

Figure 2. Overview of the dwarf galaxy detection and characterization pipeline. *Green* indicates completed stages, *orange* indicates current development.

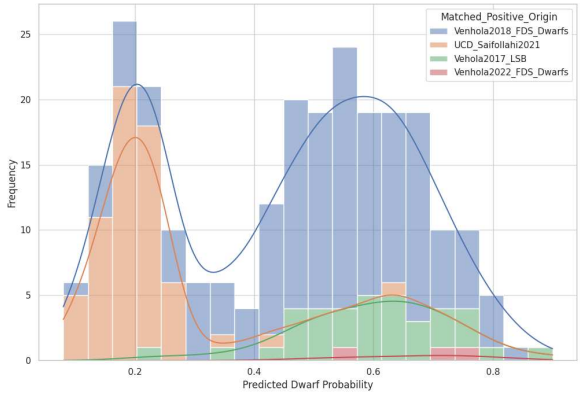

Figure 3. Probability distribution of dwarf candidates predicted by the Random Forest classifier.

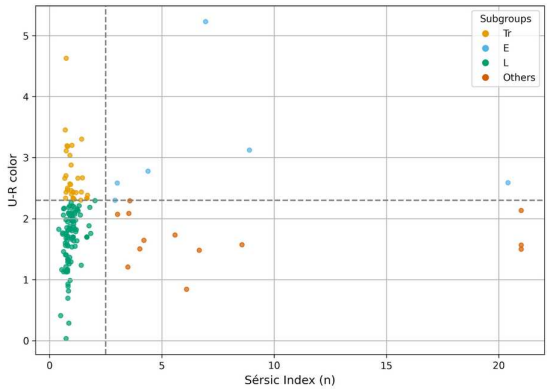

Figure 4. Structural and photometric properties of the detected dwarf candidates. Most candidates appear diffuse and blue, though these results are preliminary.

learned by the classifier (e.g. stars vs. galaxies, bright vs. faint, or compact vs. extended objects). Its physical meaning, however, requires a focused inspection of the sources contributing to each peak.

4. Preliminary Characterization of Detected Candidates

After running the pipeline on the test fields, we examined the structural and photometric properties of the recovered sources to obtain an initial view of the objects it selects.

4.1. Structural and Photometric Properties

Structural parameters were measured with `Morfometrika` (Ferrari et al. 2015). Figure 4 shows the $u - r$ versus Sérsic index (n) distribution, with reference divisions at $u - r = 2.3$ and $n = 2.5$ from Vika et al. (2015) and Montaguth et al. (2025), which separate the parameter space into regions broadly associated with early-type (E), late-type (L), transition (Tr), and mixed or unclassified systems.

While this parameter space provides a useful first-order framework, these relations were calibrated for larger, well-resolved galaxies and should be applied to dwarf systems with caution, particularly given the presence of unusually high n values likely driven by fitting uncertainties in faint and low–surface–brightness objects. Most detections populate the low-n, blue region of the diagram, consistent with the expected locus of diffuse, irregular, and star-forming dwarf galaxies, indicating that the recovered candidates occupy the standard dwarf regime without introducing obvious structural selection biases.

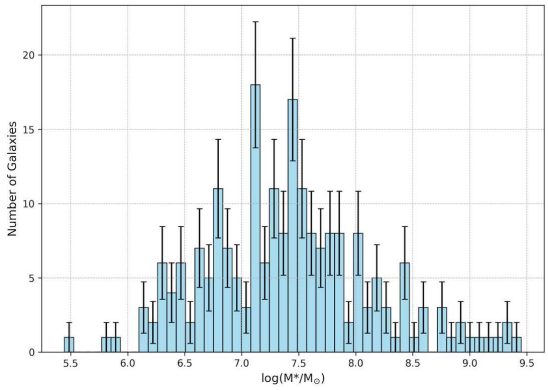

Figure 5. Preliminary stellar mass distribution of detected candidates.

4.2. Stellar Mass Estimates

Stellar masses were estimated using the empirical relation from Taylor et al. 2011:

$$\log M_*/[M_\odot] = -0.68 + 0.70(g - i) - 0.4\, M_i, \qquad (2)$$

where M_i is the absolute i-band magnitude and $(g-i)$ the rest-frame color. Figure 5 shows that stellar masses are $\log(M_*/M_\odot) \sim$ 5.5–9.9.

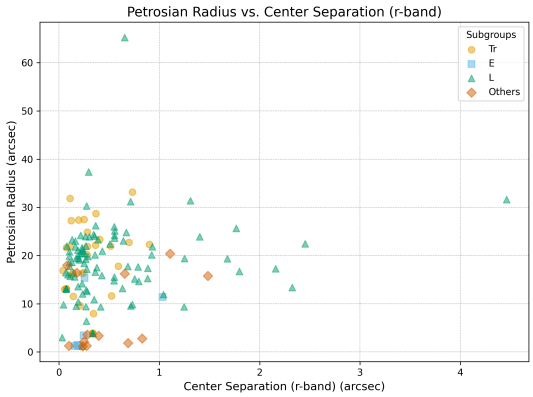

Figure 6. Offset between center of light and center of mass. Larger offsets are mostly seen in late-type galaxies.

4.3. Center of Light vs Center of Mass

We compared the center of light with the center of mass, derived from morfometrika, for each candidate which is shown in Figure 6. Most objects show small offsets, but a few, mainly late-type dwarfs, exhibit shifts up to 2.5 arcsec, likely due to structural asymmetries or tidal features. Such offsets can indicate environmental influence on galaxy morphology.

5. Future Work

Following the preliminary detection of dwarf galaxies in S-PLUS, the next steps of this project include the application of the detection pipeline to the deeper DECaLS imaging to identify fainter systems not detectable in S-PLUS, followed by cross-survey validation to assess completeness and photometric consistency between the two datasets. High-probability dwarf candidates will then be subjected to detailed structural and environmental analyses using Morfometrika and complementary tools. In parallel, simulated galaxy injections will be used to quantify detection completeness and validate photometric measurements. Finally, the methodology will be extended to a larger sample of 36 galaxy clusters observed by S-PLUS, enabling systematic studies of dwarf galaxy populations across environments comparable to Fornax.

References

Annibali, F. & Tosi, M. 2022, Universe, 8, 52
Avila, F. et al. 2018, JCAP, 12, 041
Avila, F. et al. 2022, MNRAS, 509, 2994
Avila, F. et al. 2023, Braz. J. Phys., 53, 49
Bertin, E. & Arnouts, S. 1996, A&AS, 117, 393
Besla, G. et al. 2012, MNRAS, 421, 2109
Binggeli, B., Sandage, A. & Tammann, G. A. 1985, AJ, 90, 1681
Boselli, A., Gavazzi, G. & Boissier, S. 2006, in SF2A-2006, ed. D. Barret et al., 317
Boselli, A. & Gavazzi, G. 2014, A&ARv, 22, 74
Dark Energy Survey Collaboration et al. 2018, ApJS, 239, 18
Davis, M. et al. 2015, ApJ, 292, 371
Dey, A. et al. 2019, AJ, 157, 168
Dressler, A. 1980, ApJ, 236, 351
Eigenthaler, P. et al. 2018, ApJ, 855, 142
Famaey, B. & McGaugh, S. S. 2012, Living Rev. Relativ., 15, 10
Fattahi, A. et al. 2018, MNRAS, 476, 3816
Ferrari, F., de Carvalho, R. R. & Trevisan, M. 2015, ApJ, 814, 55
Gnedin, O. Y. 2003, ApJ, 582, 141
Haack, R. F. et al. 2024, MNRAS, 530, 3195
Häußler, B. et al. 2022, A&A, 664, A92
Ibata, R. A., Gilmore, G. & Irwin, M. J. 1994, Nature, 370, 194
Jaffé, Y. L. et al. 2018, MNRAS, 476, 4753
Mendes de Oliveira, C. et al. 2019, MNRAS, 489, 241
Merritt, D. 1983, ApJ, 264, 24
Milgrom, M. 1983, ApJ, 270, 365
Montaguth, G. P. et al. 2025, A&A, 696, A240
Moore, B. et al. 1996, Nature, 379, 613
Moore, B., Lake, G. & Katz, N. 1998, ApJ, 495, 139
Müller, O. & Crosby, E. 2023, A&A, 677, A19
Peñarrubia, J., Navarro, J. F. & McConnachie, A. W. 2008, ApJ, 673, 226
Peng, Y.-j. et al. 2010, ApJ, 721, 193
Peng, Y.-j. et al. 2012, ApJ, 757, 4
Romanowsky, A. J. et al. 2024, ApJL, 964, L14
Saifollahi, T. et al. 2021, MNRAS, 504, 3580
Smith, R. et al. 2013, MNRAS, 429, 1066
Smith Castelli, A. V. et al. 2024, MNRAS, 530, 3787
Springel, V. et al. 2005, Nature, 435, 629
Taylor, E. N. et al. 2011, MNRAS, 418, 1587
Venhola, A. et al. 2017, A&A, 608, A142
Venhola, A. et al. 2018, A&A, 620, A165
Venhola, A. et al. 2022, A&A, 662, A43
Vika, M. et al. 2015, A&A, 577, A97
Wang, J. et al. 2023, ApJ, 959, 72
White, S. D. M. & Rees, M. J. 1978, MNRAS, 183, 341
White, S. D. M. & Frenk, C. S. 1991, ApJ, 379, 52
Zaritsky, D. et al. 2023, ApJS, 267, 27